Industrial Chemistry & Materials

ROYAL SOCIETY OF CHEMISTRY

PAPER

View Article Online
View Journal | View Issue

Cite this: *Ind. Chem. Mater.*, 2024, **2**, 340

Uncovering gold nanoparticle synthesis using a microchip laser system through pulsed laser ablation in aqueous solution†

Barana Sandakelum Hettiarachchi, [a] Yusuke Takaoka,[b] Yuta Uetake, [ac] Yumi Yakiyama, *[ac] Hwan Hong Lim,[d] Takunori Taira,[de] Mihoko Maruyama,[f] Yusuke Mori,[f] Hiroshi Y. Yoshikawa[b] and Hidehiro Sakurai *[ac]

The synthesis of gold nanoparticles (Au NPs) was carried out by utilising the pulsed laser ablation in liquids (PLAL) method with a microchip laser (MCL) system. This portable system features low power consumption and a giant-pulse laser. Aqueous solutions with and without the surfactant poly(*N*-vinyl-2-pyrrolidone) (PVP) were used for laser ablation of a bulk gold rod to achieve the successful formation of a colloidal solution of Au NPs. The gas bubbles formed by heating the aqueous medium around the surface of the gold target significantly reduced the efficiency of Au NP ablation. This effect was more pronounced and prolonged in high-viscosity solutions, hindering energy transfer from subsequent laser pulses to the target. Additionally, it was suggested that the chain length of PVP does not affect either the size of the Au NPs or the ablation efficiency. Videography experiments were conducted to explore the ablation mechanism employed by the MCL system. The relatively short pulse duration of the MCL system may contribute to the formation of NPs with consistent size, which were suppressed to grow in significantly smaller cavitation bubbles with short lifetimes.

Received 19th August 2023,
Accepted 16th November 2023

DOI: 10.1039/d3im00090g

rsc.li/icm

Keywords: Pulsed laser ablation in liquids (PLAL); Microchip laser (MCL); Gold nanoparticles; Viscosity; Poly(*N*-vinyl-2-pyrrolidone) (PVP).

1 Introduction

Pulsed laser ablation in liquid (PLAL) has emerged as a reliable and versatile technique for producing metal nanoparticles (NPs) in solution.[1–3] Unlike conventional methods that rely on metal ion precursors, PLAL offers an environmentally friendly approach for obtaining high-purity metal NPs. This unique advantage has led to the widespread adoption of PLAL across various scientific and industrial research domains. One bottleneck in the implementation of the PLAL method in a laboratory, which is not special in laser science such as the one working on the pure organic synthesis, is introducing the laser sources and their maintenance costs. To make the utilisation of laser techniques more commonplace, Taira *et al.* have developed very compact low-power-consumption giant-pulse microchip lasers (MCLs), which are pumped by diode lasers (LDs) (Fig. 1a and S1, ESI†).[4–10] The

[a] *Division of Applied Chemistry, Graduate School of Engineering, Osaka University, 2-1 Yamadaoka, Suita, Osaka 565-0871, Japan.*
E-mail: yakiyama@chem.eng.osaka-u.ac.jp, hsakurai@chem.eng.osaka-u.ac.jp
[b] *Division of Applied Physics, Graduate School of Engineering, Osaka University, 2-1 Yamadaoka, Suita, Osaka 565-0871, Japan*
[c] *Innovative Catalysis Science Division, Institute for Open and Transdisciplinary Research Initiatives (ICS-OTRI), Osaka University, 2-1 Yamadaoka, Suita, Osaka 565-0871, Japan*
[d] *Division of Research Innovation and Collaboration, Institute for Molecular Science, 38 Nishigonaka, Myodaiji, Okazaki 444-8585, Japan*
[e] *Laser-Driven Electron-Acceleration Technology Group, RIKEN SPring-8 Center, 1-1-1 Kouto, Sayo-cho, Sayo-gun, Hyogo 679-5148, Japan*
[f] *Division of Electrical, Electronic and Infocommunications Engineering, Graduate School of Engineering, Osaka University, 2-1 Yamadaoka, Suita, Osaka 565-0871, Japan*

† Electronic supplementary information (ESI) available: Supporting figures, tables and the movie data during PLAL. See DOI: https://doi.org/10.1039/d3im00090g

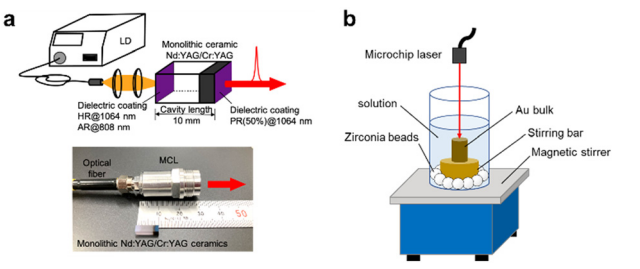

Fig. 1 Schematic models of the PLAL of Au using an MCL system. (a) Composition of the MCL system and the scale of the MCL laser head; (b) setup of PLAL system in the present research.

compactness of MCL systems makes this apparatus portable, and it occupies a only a small space.[5] In addition, strict alignment of the optical system was not required because of the cavity-coated monolithic structure of MCL,[6] lowering the barrier to entry to laser science for users without special training. Such features enable the easy and quick production of colloidal NPs in the catalytic chemistry lab, significantly accelerating the investigation of new catalytic reactions.

Additionally, recent demonstrations have highlighted that laser systems operating with a pulse duration of 1 ns achieve greater efficiency compared to those with plasma pulse durations of a few ps and >5 ns.[11–13] This is attributed to the shielding of the laser beam by the ablation plume and cavitation bubble, which occur between 1 and 5 ns after the pulse, resulting in minimal losses for PLAL. Our MCL system incorporates a short cavity length of less than 10 mm, which realises minimal pulse durations of 0.9 ns. Therefore, it is expected to achieve optimal PLAL processing in our MCL systems. Another feature of our machine is a low repetition rate of 100 Hz. Higher repetition rates can lead to a greater delivery of average power, potentially enhancing productivity.[14,15] However, they also cause more plasma and/or particle shielding, which could ultimately limit the laser ablation efficiency.[12] Thus, it remains crucial to evaluate the capability of MCL systems for PLAL of metal NPs under a short pulse duration (~1 ns) with a low repetition rate. Herein, we report a comprehensive investigation into preparing Au NPs through PLAL using MCLs in an aqueous solution with short pulse duration and a low repetition rate. We further examined the underlying ablation mechanism of this innovative MCL system. This work will contribute to the advancement of MCL utilisation, particularly in the field of chemistry.

2 Results and discussion

2.1 MCL ablation in aqueous PVP solution

Our investigation commenced with a PLAL experiment using the MCL system on a gold target in water without any stabilising surfactant. During the ablation, the colour of the solution turned from colourless to pink, reflecting the 522 nm absorption band of surface plasmon resonance (SPR) (Fig. S3, ESI†). The absorption spectra of the solution closely replicated those of Au NPs synthesised by the chemical reduction of gold salt and by PLAL with a higher-power laser source,[16–19] indicating that the present PLAL with MCL system successfully produced Au NPs. The existence of Au NPs was confirmed by TEM measurement, which gave a particle size of 4.9 ± 1.3 nm (Fig. 2). As the efficiency of MCL for the generation of Au NPs had been successfully confirmed, we next investigated the effect of the surfactant in the presence of PVP, which is often applied as a polymer-based stabilising agent for metal nanocolloids to afford a weakly bound colloidal structure *via* CT interaction between the N–C═O groups and Au.[20–22] It is known that the PVP chain length and concentration affect the resulting particle size as well as the colloid size in preparation with conventional reduction method[23] to eventually affect the catalytic ability.[24] Although PVP is commonly used as a stabilizing ligand for Au NPs in PLAL, as listed in Table 1, there has been no explicit discussion of the relationship between the polymer chain length and the resulting particle size in PLAL. This motivated us to conduct Au-targeted PLAL using our MCL system in the presence of PVP. To confirm the chain length effect of PVP, we applied three types of PVP, K-15, K-30 and K-90, with different chain lengths (M_w: 10 kDa, 40 kDa and 360 kDa, respectively) and performed PLAL in their presence in various concentrations in water. A short time after the ablation started, the colour of the PVP solution changed from colourless to a reddish tone. Subsequent TEM measurement of the resulting colloidal solutions revealed the formation of slightly smaller Au NPs in all cases than those obtained without PVP (Table 2 and S4–S6, ESI†). It was also found that the particle size was almost uniform among all the trials, indicating that the PVP chain length and concentration were not significant factors in determining the particle size. This observation was similar to a reported work,[25] while Ag NPs prepared in different PVP concentrations showed apparent differences in particle size between those prepared with and without PVP, which is explained by the improved secondary etching efficiency of the solvent-confined plasma toward the silver plate in the presence of PVP[26] (Table S1†). UV-vis spectral analysis of the colloidal solutions provided insights into the influence of PVP on PLAL using MCLs (Fig. S7, ESI†). Higher concentrations of PVP led to a reduction in the absorption intensity of the plasmonic band observed at 519 nm across all three PVP types. Moreover, the spectral shapes of the SPR bands in the colloidal solutions remained nearly identical. This effect was further validated through inductively coupled plasma-atomic emission spectroscopy (ICP-AES) measurements, which confirmed a significant decrease in the yield of Au NPs with increasing PVP concentration, regardless of the PVP chain length (Table 2). Notably, beyond a PVP concentration of 1.0×10^{-1} mol L^{-1}, a substantial decline in the quantity of the resulting Au NPs was observed.

To gain deeper insight into the relationship between PVP concentration and the yield of Au NPs, we investigated other relevant parameters. Among these parameters, viscosity stands out as one that can be influenced by the concentration of PVP. As summarised in Table 3 and Fig. 3, the experimental results revealed a distinct correlation between the yield of Au NPs and the viscosity of the reaction

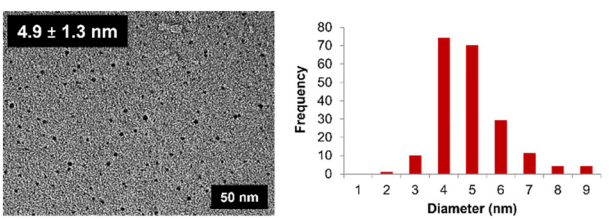

Fig. 2 TEM image and size distribution of the Au NPs produced by PLAL using the MCL in water.

Table 1 Reported sizes of Au nanoparticles generated using PLAL in the presence of PVP

PVP concentration (mol L^{-1})	Laser conditions	Particle size[a] (nm)	Ref.
0.0001[b,c], 0.001[b,c], 0.01[b,c]	100 fs, 780 nm, 10 Hz, 6 mJ per pulse	3–5	27
0.01[b,d]	100 fs, 800 nm, 1 kHz, 1 mJ per pulse	7–27	28
0.005	7 ns, 1064 nm, 10 Hz, 11 mJ per pulse	20–50[e]	25
0.4	8 ns, 335 nm, 10 Hz, 17 mJ per pulse[f]	720[g]	29

[a] TEM measurement. [b] wt%. [c] Laser ablation in $HAuCl_4$ solution. [d] Prepared by laser ablation in $KAuCl_4$ solution followed by seed-mediated growth method. [e] Hydrodynamic diameter. [f] Estimated from 0.5 mm diameter and 17 J cm^{-2} fluence. [g] Based on SEM image.

solution. To further explore this connection, we conducted PLAL experiments using solutions with a fixed viscosity (~2.2 mPa s) while varying PVP chain lengths (Table S2, ESI†). Interestingly, regardless of the specific PVP chain length employed, the quantity of ablated Au NPs remained consistent. The result strongly suggests that solution viscosity is pivotal in determining ablation efficiency in the presence of PVP.

2.2 Real-time monitoring of ablation using a high-speed camera

To comprehensively understand how solution viscosity influences ablation efficiency, we conducted PLAL experiments using a gold target under varying viscosity conditions. Real-time monitoring of the ablation process was achieved using a high-speed camera, capturing images at a rate of 4 milliseconds per frame during the initial laser ablation and five minutes thereafter. The experimental results vividly demonstrated the influence of PVP solution viscosity on the initial laser ablation stage during the production of Au NPs (Fig. 4a–d and Videos S1–S4, ESI†). When a PVP K-15 solution with lower viscosity underwent laser ablation, Au NPs were ejected and dispersed rapidly, accompanied by the generation of only a small amount of gas bubbles (Fig. 4a and Video S1, ESI†). This behaviour is attributable to the high dispersibility of gas bubbles in low-viscosity media. On the contrary, as the viscosity increased, *i.e.*, in the PVP K-15 solution with higher viscosity, the ejection rate of NPs decreased, and gas bubble dispersion became less effective (Fig. 4b and Video S2, ESI†). Under even higher viscosity conditions with PVP K-30 and PVP K-90, both the ejection rate of NPs and the dispersion of gas bubbles became considerably slower, particularly in the case of PVP K-30, which exhibited the highest viscosity (Fig. 4c and d and Videos S3 and S4, ESI†). Five minutes after the laser irradiation, the gas bubbles continued to move slowly through the solution, positioning themselves along the laser pathway in all tested conditions, although their densities were different (Fig. 4e–h and Videos S5–S8, ESI†). This phenomenon hindered the smooth energy transfer from subsequent laser pulses to the target material by absorbing, reflecting, and scattering the laser beam, as the persistent bubbles act as a shield.[30–33] These observations revealed that the solution viscosity influenced the diffusion of gas bubbles, ultimately controlling the effectiveness of the laser ablation process. It is important that the higher solution viscosity also causes a thicker stationary film on the bulk target, which accommodates generated NPs more to give satellite bubbles.[13] Another noteworthy point is that the cavitation bubble and plasma plume, which are generally formed after creating a local region with high temperature and pressure due to high-intensity laser pulse irradiation of a solid target,[34–36] were not confirmed in the present images.

Table 2 Effects of PVP concentration and chain length on Au NP size

PVP concentration[a] (mol L^{-1})	Particle size (nm)		
	PVP K-15	PVP K-30	PVP K-90
1.0×10^{-4}	4.2 ± 1.4	3.9 ± 1.2	4.3 ± 1.4
1.0×10^{-3}	3.9 ± 1.0	3.5 ± 0.9	3.9 ± 0.6
1.0×10^{-2}	3.7 ± 0.9	3.3 ± 1.0	3.6 ± 0.9
1.0×10^{-1}	3.2 ± 0.7	3.1 ± 0.7	3.5 ± 0.8
1.0	3.8 ± 1.0	3.6 ± 0.8	n.d.[b]

[a] In water (15 mL). [b] No data was obtained due to the high viscosity of the solution.

Although we adjusted the image capture frame to a shorter interval of 2 μs for a duration of 10 ms, no generation of cavitation bubble was confirmed (Fig. S8, ESI†). Considering that the second laser pulse does not affect for the cavitation bubble size as long as the repetition rate is in the range of 10–1000 Hz, the size of cavitation bubble is mainly affected by the laser fluence if the duration is comparable. Indeed, the reported works with a 1 ns duration and even a 0.4 J cm^{-2} fluence show the clear formation of the cavitation bubble.[13] As the laser fluence of our MCL system is >13.7 J cm^{-2}, it seems reasonable that a cavitation bubble formed, but was too small to be detected in our experimental setting. This may be attributable to the combination of small pulse energy and small spot size. Although there are reports about the effect of the presence of PVP[25] and viscosity,[37] the discussion is difficult to apply directly to explain our results due to the significant difference in the PVP concentration and viscosity range; in fact, the possibility that PVP affects the cavitation bubble formation was ruled out by the absence of the bubble even in the absence of PVP (Fig. S8, ESI†). Therefore, our work is quite meaningful to uncover the effects of veiled conditions on the ablation phenomenon. According to Rayleigh–Plesset theory,[38,39] such small bubbles probably had a short lifetime and thus provided only limited space for the nucleation and growth of the NPs, resulting in the relatively small and constant size of the NPs.[40] The fragmentation of initially formed relatively large NPs by

Table 3 Effects of PVP concentration and chain length on Au NP concentration

PVP concentration[a] (mol L^{-1})	PVP K-15		PVP K-30		PVP K-90	
	Au productivity (μg h^{-1})	Viscosity (mPa s)	Au productivity (μg h^{-1})	Viscosity (mPa s)	Au productivity (μg h^{-1})	Viscosity (mPa s)
1.0×10^{-4}	226	0.94 ± 0.05	236	0.94 ± 0.02	223	0.95 ± 0.05
1.0×10^{-3}	220	0.94 ± 0.04	200	0.95 ± 0.02	200	0.96 ± 0.01
1.0×10^{-2}	192	0.96 ± 0.04	196	0.96 ± 0.04	131	1.07 ± 0.02
1.0×10^{-1}	179	1.01 ± 0.02	107	1.26 ± 0.06	75	3.27 ± 0.03
1.0	104	2.32 ± 0.03	76	6.39 ± 0.03	n.d.[b]	n.d.[b]

[a] In water (15 mL). [b] No data was obtained due to the high viscosity of the solution.

the sequential laser pulses due to the long ablation time (1 h) might be another possible reason for the formation of small NPs.[41]

2.3 Relationship between the ablation efficiency and the solution viscosity in MCL ablation

In low-viscosity solutions, the bubbles diffuse and eventually disappear from the region in which they are initially generated within a specific time interval (Δt). However, in high-viscosity solutions, the density of gas bubbles remains high along the laser pathway within the same Δt due to the significant suppression of the bubble diffusion. The ablation efficiency, accounting for the presence of gas bubbles, is modelled using the three-dimensional diffusion eqn (1) based on Fick's second law.[42]

$$\frac{\partial C}{\partial t} = D\left(\frac{\partial^2 C}{\partial x^2} + \frac{\partial^2 C}{\partial y^2} + \frac{\partial^2 C}{\partial z^2}\right) \quad (1)$$

where C represents the concentration of diffused gas bubbles after time t at the three-dimensional coordinates x, y and z relative to the bubble-generating laser spot. D is the diffusion coefficient. The solution of eqn (1) is represented as eqn (2).

$$C(x,\ y,\ z,\ t) = \frac{C_0}{8(\pi D t)^{\frac{3}{2}}} \exp\left[\frac{-(x^2+y^2+z^2)}{4Dt}\right] \quad (2)$$

Here, the initial ($t = 0$) concentration of gas bubbles at the generation point on the bulk Au surface ($x = 0$, $y = 0$, $z = 0$) is denoted as C_0. If the volume to be considered is fixed as V, the total amount of gas bubbles at the specific area (x, y, z) with a volume of V at time t can be presented as eqn (3).

$$C(x,\ y,\ z,\ t)\cdot V = \frac{C_0 V}{8(\pi D t)^{\frac{3}{2}}} \exp\left[\frac{-(x^2+y^2+z^2)}{4Dt}\right] \quad (3)$$

The effect of solution viscosity on the gas bubble diffusion can be described using the Stokes–Einstein relation, which establishes a connection between the diffusion constant D and the viscosity η.[43]

$$D = k_B T/6\pi\eta R \quad (4)$$

In this equation, k_B represents the Boltzmann constant, T is the temperature, and R is the radius of the gas bubble. By rearranging, we obtain:

$$C(x,\ y,\ z,\ t)\cdot V = \frac{C_0 V}{8(\pi t k_B T/6\pi\eta R)^{\frac{3}{2}}} \exp\left[\frac{-(x^2+y^2+z^2)}{4tk_B T/6\pi\eta R}\right] \quad (5)$$

Based on the analysis of the video data and the ICP data, we assumed that the intensity of scattered light (I) is directly proportional to the number of gas bubbles and can be represented as:

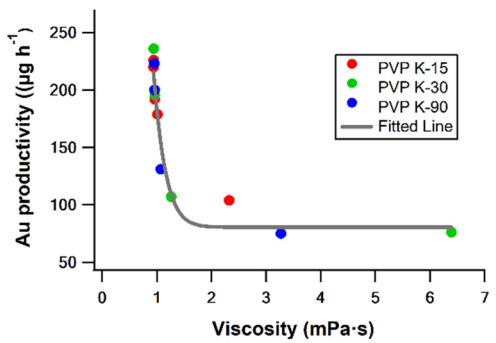

Fig. 3 Plot of the amount of Au ablated *versus* solution viscosity. The fitting curve is based on eqn (9).

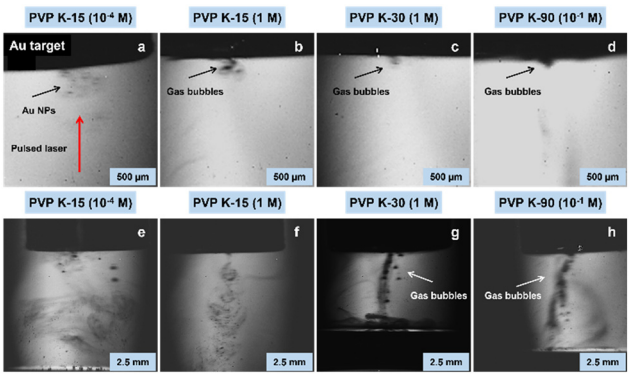

Fig. 4 Snapshot images of gas bubble accumulation along the laser irradiation pathway in PVP aqueous solutions with different viscosities. (a) and (e) PVP K-15 (0.94 mPa s); (b) and (f) PVP K-15 (2.32 mPa s); (c) and (g) PVP K-30 (6.39 mPa s); (d) and (h) PVP K-90 (3.27 mPa s). (a)–(d) were captured during the initial laser ablation at a rate of 4 ms per frame, and (e)–(h) were 5 minutes after the laser irradiation. Red arrow indicates the pulsed laser direction in (a). In this experiment, laser fluence was set to 13.7 J cm^{-2}.

$$I \propto C{\cdot}V \tag{6}$$

When certain parameters, such as temperature, refractive index, wavelength of light, bubble velocity, and shape remain constant, eqn (5) can be further simplified as:

$$C(x,\ y,\ z,\ t){\cdot}V = a(b\eta)^{\frac{3}{2}} \exp[-c\eta] \tag{7}$$

Here, a, b and c are constants. Therefore, the relationship between the intensity of scattered light and the concentration of gas bubbles at position (x, y, z) after a time interval Δt is described as:

$$I \propto a(b\eta)^{\frac{3}{2}} \exp[-c\eta] \tag{8}$$

The laser power that remains after interacting with a bubble can be described as the difference between the incident laser power (P) and the scattered light intensity, which is mathematically expressed as:

$$\text{Remaining laser power} = P - \text{scattered light intensity} \tag{9}$$

As the ablation efficiency correlates to the total laser power introduced into the system in the same instrument setting, the viscosity effect of the reaction media on the ablation efficiency is nicely rationalised by the above equations. In other words, when specific parameters, such as the temperature, refractive index, wavelength of light, bubble velocity, and shape, remain constant, the efficiency of the ablation of Au NPs decreases as the solution viscosity increases. The relationship presented in eqn (9) matches with the fitted line of the amount of Au *versus* solution viscosity in Fig. 3.

2.4 Perspectives of MCL ablation

Finally, a PLAL experiment employing both the MCL and a higher-power laser was carried out to evaluate the ablation effectiveness of MCL with the laser conditions outlined in Table 4. Although it was impossible to use the same pulse energy setting due to the great differences in the machine specifications, an investigation using a fixed total laser energy revealed the features of the MCL system. When we fixed the total applied laser power to 100 J in both settings by applying an appropriate irradiation time depending on the laser pulse energy and the spot size (769 seconds for the MCL laser and 400 seconds for the Quanta-Ray Pro-250), it was found that the MCL system produced only 101 μg h^{-1} of Au productivity, while it showed comparable ablation efficiency (0.8 mg W^{-1} h^{-1}) to that of the other system (620 μg h^{-1}, 2.5 mg W^{-1} h^{-1}) despite the approximately 20-times-lower pulse energy of the MCL system. The relatively high ablation efficiency of our MCL system was probably attributable to the effective energy transfer from each laser shot to the metal surface with a ~1 ns pulse duration without any energy shielding effect caused by the interaction with the sequential laser plume, cavitation bubbles, and generated NPs, unlike the longer pulse duration system.[12,13] This result suggested that the MCL offers environmentally friendly metal NP preparation with reduced total energy input, affording the potential benefits and practical applications of the MCL in various materials fields.

Table 4 Settings and PLAL parameters of the present MCL system and the ns-laser (Quanta-Ray PRO-250) system in a comparison experiment

	Present MCL	Quanta-Ray PRO-250
Pulse energy (mJ)	1.3	25
Pulse duration (ns)	0.9	12
Spot diameter (μm)	130 ± 6	800 ± 13
Repetition rate (Hz)	100	10
Au productivity (μg h^{-1})	101	620
Ablation efficiency (mg W^{-1} h^{-1})	0.8	2.5

3 Conclusions

We demonstrated the PLAL of bulk Au in water using an MCL with short pulse duration (0.9 ns) and a low repetition rate (100 Hz) and investigated the effect of the laser specifications with the focus on the solution viscosity, which was controlled by the concentration and/or chain length of PVP. Successful generation of Au NPs was achieved, and the particle size was relatively small (2–5 nm), which was probably due to the significantly small size of the cavitation bubble due to the small pulse energy and small spot size, although this needs to be clarified in future work. The yield of NPs was significantly affected by the solution viscosity, which controlled the gas bubble diffusion to affect the laser energy transfer to the system. Although the low repetition rate gave a small AuNP yield, the short 0.9 ns pulse duration suppressed the energy shielding effect to realise relatively high ablation efficiency despite having a much smaller pulse energy than the other system. This study provides new insights into the preparation of Au NPs with a compact MCL system and affords the capability to install an MCL in standard synthetic chemistry laboratories.

4 Experiments

4.1 General

All reagents purchased from commercial suppliers were used without further purification unless otherwise noted. Ultrapure water (18.2 Ω cm^{-1}) was produced by an Organo Puric-ω water purification system. Transmission electron microscopy (TEM) images were recorded with a JEOL JEM-2100 electron microscope at an accelerating voltage of 200 kV using a Holey carbon support film coated Cu microgrid (EMJapan, U1003). Before use, the TEM grid underwent hydrophilic treatment in a glow discharge irradiation chamber. The obtained TEM images were analysed using Image-J software, and the expressed mean diameter and standard deviation are based on the average of 300 particles. Inductively coupled plasma atomic emission spectroscopy (ICP-AES) was conducted using a Shimadzu ICPS-8100.

Viscosity measurements were performed with a HAAKE RheoStress 6000 (Thermo Scientific) running at a shear rate of 1000 s^{-1} at 25 °C. There was no significant variation between the viscosity values pre- and post-PLAL, so all viscosity measurements were taken before PLAL.

4.2 MCL specifications

The MCL comprised a monolithic Nd:YAG/Cr^{4+}:YAG ceramic with a dimension of 3 × 3 × 10 mm^3. The Nd-doping rate and the initial transmittance of Cr^{4+}:YAG were 1.1 at% and 30%, respectively. The input surface was dual-coated for anti-reflection (AR) at 808 nm for end-pump and high-reflection (HR) at 1064 nm for laser oscillation. The output surface was 50% partial reflection (PR)-coated for the same laser wavelength. The monolithic ceramic was set in a metal module with two lenses for the fibre-coupled pump. The MCL generated laser pulses with a >0.5 MW peak power (pulse energy of 0.5 mJ and a pulse duration of 900 ps) at 100 Hz (average power of 50 mW) without active cooling.[7,9]

4.3 General PLAL method

A gold target (>99.99%, 5 × 15 mm) was cleaned by ultrasonication in acetone for 5 min and rinsed with deionised water before use. The target was fixed on a custom laboratory-built holder (PEEK) equipped with a magnetic stir bar, which was then placed at the bottom of a Pyrex® vessel (30 × 80 mm). An appropriate number of zirconia beads (φ 6 mm) were placed between the vessel and the holder to prevent the axis of rotation from moving (Fig. 1b). To this was added 15 mL of an aqueous solution containing poly(*N*-vinyl-2-pyrrolidone) (PVP) (K-15: 10 kDa, K-30: 40 kDa, K-90: 360 kDa) with a concentration of 10^{-4} mol L^{-1}, 10^{-3} mol L^{-1}, 10^{-2} mol L^{-1}, 10^{-1} mol L^{-1}, and 1 mol L^{-1}, as well as the fixed viscosity PVP solutions (~2.2 mPa s), which consisted of 1 mol L^{-1}, 0.42 mol L^{-1} and 0.07 mol L^{-1} PVP K-15, K-30 and K-90, respectively. After that, the pulsed laser was used to irradiate the gold target at room temperature for 60 min, with stirring at 200 rpm. The thus-obtained Au : PVP was applied for further analyses. For all the experiments, the same parameter settings were used. The microchip laser parameters were adjusted to the following conditions for the experiment: wavelength of 1064 nm, pulse energy of 1.8 mJ, pulse duration of 900 ps, peak power of >2 MW, and a repetition rate of 100 Hz with an average power of 180 mW.

4.4 Investigation of bubble formation and ablation mechanism using high-speed camera

A high-speed camera (HPV-2, Shimadzu Corporation, 312 × 260 pixels, maximum frame rate = 1000 kfps) was synchronised with the MCL *via* a function generator (Wave Factory, WF1943). One hundred images were recorded for MCL ablation using different frame intervals: 4 ms for the solution viscosity experiment and 2 μs for investigating the PLAL mechanism using MCL. The gold sample was observed through an objective lens (Olympus, 2×, NA, 0.06) in front of the camera. An LED light source (THORLABS, DC20) was used for illumination. The liquid level was set to 5 mm above the gold surface. The laser beam was directly focused on the target surface. The detailed settings are depicted in Fig. S2, ESI.† The average spot diameter at the laser focus (130 ± 6 μm) was measured by ablating black ink on a glass substrate in air, corresponding to a nominal laser fluence of 13.7 J cm^{-2} (pulse energy: 1.3 mJ per pulse). For comparison, an experiment using a Nd:YAG laser was operated using a Quanta-Ray PRO-250 (wavelength, 1064 nm; pulse energy, 1500 mJ; pulse duration, 12 ns; peak power, 125 MW; average laser power, 15 W; repetition rate, 10 Hz). For the experiment, the laser parameters were set as follows: wavelength, 1064 nm; pulse energy, 25 mJ; pulse duration, 12 ns; repetition rate, 10 Hz.

Conflicts of interest

There are no conflicts to declare.

Acknowledgements

This study was supported by JSPS KAKENHI (JP19K22187). Y. Y. and H. Y. Y. acknowledge Amada Foundation for the Promotion of Science & Engineering for financial support. B. S. H. thanks the Japan International Cooperation Agency (JICA) and Otsuka Toshimi Scholarship Foundation (21-S58 and 22-S30) for kindly providing scholarships. We thank Prof. Taka-aki Asoh (Tokyo Univ. Sci.) and Prof. Satoshi Seino (Osaka Univ.) for their support with viscosity and TEM measurements, respectively.

References

1 D. Zhang, Z. Li and K. Sugioka, Laser ablation in liquids for nanomaterial synthesis: Diversities of targets and liquids, *JPhys Photonics*, 2021, **3**, 042002.
2 D. Zhang, B. Gökce and S. Barcikowski, Laser synthesis and processing of colloids: Fundamentals and applications, *Chem. Rev.*, 2017, **117**, 3990–4103.
3 M. Kim, S. Osone, T. Kim, H. Higashi and T. Seto, Synthesis of nanoparticles by laser ablation: A review, *Kona Powder Part. J.*, 2017, **34**, 80–90.
4 J. J. Zayhowski and A. Mooradian, Frequency-modulated Nd:YAG microchip lasers, *Opt. Lett.*, 1989, **14**, 618–620.
5 J. J. Zayhowski, J. Ochoa and A. Mooradian, Gain-switched pulsed operation of microchip lasers, *Opt. Lett.*, 1989, **14**, 1318–1320.
6 T. Taira, A. Mukai, Y. Nozawa and T. Kobayashi, Single-mode oscillation of laser-diode-pumped Nd:YVO4 microchip lasers, *Opt. Lett.*, 1991, **16**, 1955–1957.
7 T. Taira, RE^{3+}-ion-doped YAG ceramic lasers, *IEEE J. Sel. Top. Quantum Electron.*, 2007, **13**, 798–809.
8 H. Sakai, H. Kan and T. Taira, >1 MW peak power single-mode high-brightness passively Q-switched Nd^{3+}:YAG microchip laser, *Opt. Express*, 2008, **16**, 19891–19899.

9 T. Taira, Domain-controlled laser ceramics toward Giant Micro-photonics, *Opt. Mater. Express*, 2011, **1**, 1040–1050.
10 H. H. Lim and T. Taira, >50 MW peak power, high brightness Nd:YAG/Cr^{4+}:YAG microchip laser with unstable resonator, *Opt. Express*, 2022, **30**, 5151–5158.
11 S. Dittrich, M. Spellauge, S. Barcikowski, H. P. Huber and B. Gokce, Time resolved studies reveal the origin of the unparalleled high efficiency of one nanosecond laser ablation in liquids, *Opto-Electron. Adv.*, 2022, **5**, 210053.
12 S. Dittrich, R. Streubel, C. McDonnell, H. P. Huber, S. Barcikowski and B. Gokce, Comparison of the productivity and ablation efficiency of different laser classes for laser ablation of gold in water and air, *Appl. Phys. A: Mater. Sci. Process.*, 2019, **125**, 432.
13 S. Dittrich, S. Barcikowski and B. Gokce, Plasma and nanoparticle shielding during pulsed laser ablation in liquids cause ablation efficiency decrease, *Opto-Electron. Adv.*, 2021, **4**, 200072.
14 G. Raciukaitis, M. Brikas, P. Gecys and M. Gedvilas, Accumulation effects in laser ablation of metals with high-repetition-rate, *Proc. SPIE*, 2008, 7005.
15 R. Streubel, S. Barcikowski and B. Gokce, Continuous multigram nanoparticle synthesis by high-power, high-repetition-rate ultrafast laser ablation in liquids, *Opt. Lett.*, 2016, **41**, 1486–1489.
16 J. Liu, W. Ong, E. Román, M. J. Lynn and A. E. Kaifer, Cyclodextrin-modified gold nanospheres, *Langmuir*, 2000, **16**, 3000–3002.
17 M. M. Alvarez, J. T. Khoury, T. G. Schaaff, M. N. Shafigullin, I. Vezmar and R. L. Whetten, Optical absorption spectra of nanocrystal gold molecules, *J. Phys. Chem. B*, 1997, **101**, 3706.
18 F. Mafuné, J. Kohno, Y. Takeda, T. Kondow and H. Sawabe, Formation of gold nanoparticles by laser ablation in aqueous solution of surfactant, *J. Phys. Chem. B*, 2001, **105**, 5114–5120.
19 F. Mafuné, J. Kohno, Y. Takeda and T. Kondow, Formation of gold nanonetworks and small gold nanoparticles by irradiation of intense pulsed laser onto gold nanoparticles, *J. Phys. Chem. B*, 2003, **107**, 12589–12596.
20 H. Tsunoyama, H. Sakurai, N. Ichikuni, Y. Negishi and T. Tsukuda, Colloidal gold nanoparticles as catalyst for carbon –carbon bond formation: Application to aerobic homocoupling of phenylboronic acid in water, *Langmuir*, 2004, **20**, 11293–11296.
21 M. Okumura, Y. Kitagawa, T. Kawakami and M. Haruta, Theoretical investigation of the hetero-junction effect in PVP stabilized Au_{13} clusters. The role of PVP in their catalytic activities, *Chem. Phys. Lett.*, 2008, **459**, 133–136.
22 H. Tsunoyama, N. Ichikuni, H. Sakurai and T. Tsukuda, Effect of electronic structures of Au clusters stabilized by poly(N-vinyl 2-pyrrolidone) on aerobic oxidation catalysis, *J. Am. Chem. Soc.*, 2009, **131**, 7086–7093.
23 J. Li, K. Inukai, Y. Takahashi, A. Tsuruta and W. Shin, Effect of PVP on the synthesis of high-dispersion core–shell barium-titanate–polyvinylpyrrolidone nanoparticles, *J. Asian Ceram. Soc.*, 2017, **5**, 216–225.
24 S. Haesuwannakij, T. Kimura, Y. Furutani, K. Okumura, K. Kokubo, T. Sakata, H. Yasuda, Y. Yakiyama and H. Sakurai, The impact of the polymer chain length on the catalytic activity of poly(n-vinyl-2-pyrrolidone)-supported gold nanoclusters, *Sci. Rep.*, 2017, **7**, 9579.
25 A. Letzel, S. Reich, T. dos Santos Rolo, A. Kanitz, J. Hoppius, A. Rack, M. P. Olbinado, A. Ostendorf, B. Gökce, A. Plech and S. Barcikowski, Time and mechanism of nanoparticle functionalization by macromolecular ligands during pulsed laser ablation in liquids, *Langmuir*, 2019, **35**, 3038–3047.
26 T. Tsuji, D.-H. Thang, Y. Okazaki, M. Nakanishi, Y. Tsuboi and M. Tsuji, Preparation of silver nanoparticles by laser ablation in polyvinylpyrrolidone solutions, *Appl. Surf. Sci.*, 2008, **254**, 5224–5230.
27 T. Nakamura, Y. Mochidzuki and S. Sato, Fabrication of gold nanoparticles in intense optical field by femtosecond laser irradiation of aqueous solution, *J. Mater. Res.*, 2008, **23**, 968–974.
28 A. N. Hidayah, D. Triyono, Y. Herbani and R. Saleh, Tuning size and shape of gold nanoparticles using seed-mediated growth by unfocused femtosecond laser-induced plasma, *Opt. Lett.*, 2023, **48**, 2126–2129.
29 J. Larez, R. Castell and C. Rojas, Colloids and composite materials Au/PVP and Ag/PVP generated by laser ablation in polymeric liquid environment, *Rev. Mex. Fis.*, 2016, **62**, 188–192.
30 M.-R. Kalus, N. Bärsch, R. Streubel, E. Gökce, S. Barcikowski and B. Gökce, How persistent microbubbles shield nanoparticle productivity in laser synthesis of colloids-quantification of their volume, dwell dynamics, and gas composition, *Phys. Chem. Chem. Phys.*, 2017, **19**, 7112–7123.
31 S. Reich, P. Schönfeld, A. Letzel, S. Kohsakowski, M. Olbinado, B. Gökce, S. Barcikowski and A. Plech, Fluence threshold behaviour on ablation and bubble formation in pulsed laser ablation in liquids, *ChemPhysChem*, 2017, **18**, 1084–1090.
32 T. Hupfeld, G. Laurens, S. Merabia, S. Barcikowski, B. Gökce and D. Amans, Dynamics of laser-induced cavitation bubbles at a solid–liquid interface in high viscosity and high capillary number regimes, *J. Appl. Phys.*, 2020, **127**, 044306.
33 M.-R. Kalus, R. Lanyumba, S. Barcikowski and B. Gökce, Discrimination of ablation, shielding, and interface layer effects on the steady-state formation of persistent bubbles under liquid flow conditions during laser synthesis of colloids, *J. Flow Chem.*, 2021, **11**, 773–792.
34 M. Spellauge, C. Donate-Buendía, S. Barcikowski, B. Gokce and H. P. Huber, Comparison of ultrashort pulse ablation of gold in air and water by time-resolved experiments, *Light: Sci. Appl.*, 2022, **11**, 68.
35 L. V. Zhigilei, Z. Lin and D. S. Ivanov, Atomistic modeling of short pulse laser ablation of metals: Connections between melting, spallation, and phase explosion, *J. Phys. Chem. C*, 2009, **113**, 11892–11906.

36 M. Senegacnik, K. Kunimoto, S. Yamaguchi, K. Kimura, T. Sakka and P. Gregorcic, Dynamics of laser-induced cavitation bubble during expansion over sharp-edge geometry submerged in liquid– An inside view by diffuse illumination, *Ultrason. Sonochem.*, 2021, **73**, 105460.
37 K. Mehta, S. Soumyashree, J. Pandya, P. Singh, R. K. Kushawaha, P. Kumar, S. Shinde, J. Saha and P. K. Baruah, Impact of viscosity of liquid on nanoparticles synthesized by laser ablation in liquid: An experimental and theoretical investigation, *Appl. Phys. A: Mater. Sci. Process.*, 2023, **129**, 388.
38 K. Oguchi, M. Enoki and N. Hirata, Numerical simulation for cavitation bubble near free surface and rigid boundary, *Mater. Trans.*, 2015, **56**, 534–538.
39 A. Vogel, S. Busch and U. Parlitz, Shock wave emission and cavitation bubble generation by picosecond and nanosecond optical breakdown in water, *J. Acoust. Soc. Am.*, 1996, **100**, 148.
40 W. Soliman, N. Takeda and K. Sasaki, Growth processes of nanoparticles in liquid-phase laser ablation studied by laser-light scattering, *Appl. Phys. Express*, 2010, **3**, 35201.
41 F. Mafuné, J. Kohno, Y. Takeda and T. Kondow, Dissociation and aggregation of gold nanoparticles under laser irradiation, *J. Phys. Chem. B*, 2001, **105**, 9050–9056.
42 J. Crank, *The mathematics of diffusion*, Oxford Univ. Press, London, 1957, p. 11.
43 L. Costigliola, D. M. Heyes, T. B. Schrøder and J. C. Dyre, Revisiting the Stokes-Einstein relation without a hydrodynamic diameter, *J. Chem. Phys.*, 2019, **150**, 021101.